Jurnal Teknologi

Full paper

A Review of Snake Models in Medical MR Image Segmentation

Mohammed Sabbih Hamoud Al-Tamimi*, Ghazali Sulong

Faculty of Computing, University Technology Malaysia, 81100 UTM Johor Bahru, Johor Malaysia

*Corresponding author: m_altamimi75@yahoo.com

Article history

Received :1 January 2014
Received in revised form :
15 February 2014
Accepted :18 March 2014

Graphical abstract

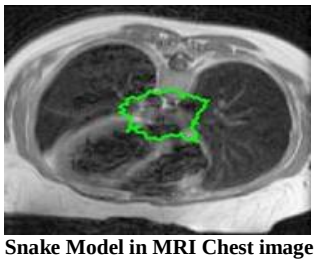

Snake Model in MRI Chest image

Abstract

Developing an efficient algorithm for automated Magnetic Resonance Imaging (MRI) segmentation to characterize tumor abnormalities in an accurate and reproducible manner is ever demanding. This paper presents an overview of the recent development and challenges of the energy minimizing active contour segmentation model called snake for the MRI. This model is successfully used in contour detection for object recognition, computer vision and graphics as well as biomedical image processing including X-ray, MRI and Ultrasound images. Snakes being deformable well-defined curves in the image domain can move under the influence of internal forces and external forces are subsequently derived from the image data. We underscore a critical appraisal of the current status of semi-automated and automated methods for the segmentation of MR images with important issues and terminologies. Advantages and disadvantages of various segmentation methods with salient features and their relevancies are also cited.

Keywords: Deformable models; active contour; snake; magnetic resonance imaging; image segmentation

1.0 INTRODUCTION

Despite the availability of different treatment options for tumor, MRI and Computer Tomography (CT) scanning are the two most common techniques used to confirm the presence of tumor and to identify the location for treatment. The choices in tumor treatment options including surgery, radiation therapy and chemotherapy often depend on the size, type and the grade of tumors. It also depends on whether or not the tumor is triggering pressure on vital parts of the human body. The possible side effects on the patients overall health caused by the spreading of the tumor to other parts of the Central Nervous System (CNS) or body are important considerations when deciding the treatment options [1].

Precise detection of the type of abnormality is highly essential for treatment planning in order to minimize diagnostic errors. The accuracy can be improved by using Computer Aided Diagnosis (CAD) systems. CAD provides an output as a second opinion to assist radiologists' image interpretation and thereby reduces image reading time. This significantly improves the accuracy and consistency of radiological diagnosis. Nonetheless, segmentation of the tumors image is very tricky task. Firstly, the variation in shapes and sizes of tumor types are quite complex [2]. Secondly, the occurrence of tumors at different locations in the human body with different image intensities is the other factor that makes automated tumor image detection and segmentation extremely difficult [1].

Image segmentation being a process of identifying and grouping image features with similar properties often solves problems via statistical classification, thresholding, edge detection, region detection or any combination of these methods. These techniques are developed on the basis of region, threshold, edge or connectivity [3]. The region based methods rely on the intensity of regular patterns within a cluster (region) of surrounding pixels. The main goal of the segmentation algorithm is to group regions rooted in their functional or anatomical characters and the performance depends on the local pixel information. It is helpful when the intensity levels of the objects fall straight outside of the range of levels in the background. Ignoring the spatial information of an image may cause problem at blurred boundary regions. The edge-based techniques depend on the discontinuation in image values between distinct regions and the main focus of segmentation algorithm here is to accurately detect the boundary that separates these regions. Conversely, the connectivity-based techniques depend on a curve known as active contour which is formed through several control points on the image.

Active models or deformable models are extensively used in image segmentations and objects tracking [4-13]. Despite many modified version of active models the active contours and active surfaces are the most popular one [4, 5, 14-17]. The active models deform the image domain to capture the desired features and minimize energy functional subjected to certain constraints. Generally, the energy function consists of an internal energy stopping the smoothness and tautness of the model and an external energy that attracts the elastic model to the features of interest. Kass *et al*. introduced the celebrated active contour model popularly known as **"Snakes"** or **"energy-minimizing curves"** [4].

This paper focuses on the importance and potential of snake models for precise detection and diagnosis of tumors through MRI

image segmentation. We conclude with a discussion on the present challenges and future promises of these models for MR image segmentation.

■2.0 PRINCIPLES OF MRI AND TUMORS CHARACTERISTICS

Varieties of imaging techniques including MRI, CT, Positron Emission Tomography (PET), Single Photon Emission Computer Tomography (SPECT) and Cerebral Angiography (CA) are developed to diagnose body tumors. Lately, CT and MRI methods are extensively employed because of their widespread availability and capability in producing high resolution images for normal anatomic structures and pathological tissues. MRI is viable in visualizing pathological or other physiological alterations of living tissues and commonly used for tumor imaging due to many advantages [18, 19]. Firstly, it does not use ionizing radiation like CT, SPECT and PET. Secondly, contrast resolution of MRI is much higher than other methods. Finally, the ability of MRI devices in generating 3D space images achieves superior tumor localization enabling the acquisition of both functional and anatomical information of the tumor during the same scan.

It is worth mentioning the working principle of MRI in addition to the image characteristics of human tumors. MRI is primarily used in medical settings to produce high quality images of the interior of the human body. As shown in Figure 1, during MR imaging, the patient is placed in a strong magnetic field which causes the protons in the water molecule of the body to align in either parallel (low energy) or anti-parallel (high energy) orientation with respect to the magnetic field. A radio frequency pulse is then introduced which forces the spinning protons to move out of equilibrium state. Upon stopping the radio frequency pulse, protons return to the equilibrium state producing a sinusoidal signal whose frequency depends on the strength of the local magnetic field. Finally, radio frequency coils or resonators within the scanner detect the signal and build the image [20, 21].

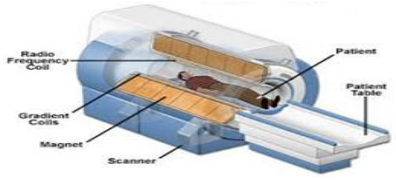

Figure 1 MRI scanner cutaway [22]

In MRI the signal processing considers signal emissions and are characterized by various magnetic signals weighting with a particular value of the echo time (Tg) and the repetition time (Tr). The signal processing has three different images such as T1-weighted, T2-weighted and PD-weighted (proton density) that can be accomplished from the patient.

Figure 2 displays typical MRI examination report of a patient's brain in three different clinical diagnosis plans including plane, sagittal plane and coronal plane. Furthermore, T1-weighted brain images from various planes are shown in Figure 2(a), (b) and (c). Depending on the type of echo recorded, there are two main families of MRI sequences namely Spin Echo (SE) and Gradient Echo (GE). SE sequence with its variant Fast Spin Echo (FSE) is established as standard MRI pulse sequences for anatomical and pathological details [23].

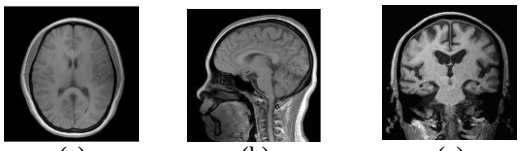

(a) (b) (c)

Figure 2 MR images from three viewpoints (a) Axial plane, (b) Sagittal plane and (c) Coronal plane [20]

Body images in MRI scan can be normal or abnormal. The abnormality is usually associated with active tumor, necrosis and edema in addition to normal body tissues. Necrosis is a dead cell located inside an active tumor, while edema is positioned near active tumor borders. Edemas are resulted from the local disruption of blood body barrier and often overlap with normal tissues that always make them difficult to distinguish from the other tissues [1].

An image from MRI scan is composed of gray level intensity values in the pixel spaces. The gray level intensity values depend on the cell concentration in the scanned volume. The darker region signifies the presence of notable abnormality.

In normal brain MR images for instance, image intensity level for brain tissues is of increasing brightness as illustrated in Figure 3. Conversely, the MR images for tumorous brain tissues depending on the type of tumor exhibit different intensity level on T1-w and T2-w images. For most tumors T1-w reveals low or intermediate signal intensity but interestingly, some tumors exhibit high signal intensity. In contrast, on T2-w most tumors display bright intensity but some disclose low intensity, the classic examples are lymphoma tumors [1]. Figure 4 shows some example of tumors intensity level characteristics in MRI.

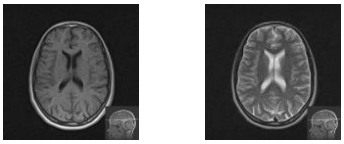

Figure 3 Original raw MRI data from pioneer diagnostic center. (a) T1-w Axial scan image and (b) T2-w Axial scan image [20]

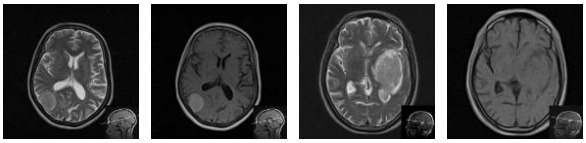

(a) (b) (c) (d)

Figure 4 Original MRI data from pioneer diagnostic center showing tumor region intensity characteristics, (a) Low intensity (T2-w) (b) High intensity (T1-w), (c) High intensity (T2-w) and (d) Low intensity (T1-w) [20]

■3.0 DIFFICULTIES IN SEGMENTATION OF MRI

Cortical segmentation has not yet been fully automated and operated at high speed. The reliability of the MRI with regards to the homogeneity of magnetic field is still debatable. The dilemmas of MRI including noise, shading artifact and partial volume effect need to be minimized. The random noise connected to MR imaging system obeying Rician distribution requires thorough realization [24]. The intensity inhomogeneity called bias field or shading artifact is the non-uniformity in the Radio Frequency (RF) field resulting shading effect during data collection is not fully understood [25]. Partial volume effect

originates when more than one type or class of tissue occupies one pixel or voxel (called mixels) of an image [26].

Segmentations of MRI outputs are normally done by medical experts requiring time consuming processes. The images of tumor tissues from different patients contain many diverse appearance and gray level intensities. They frequently look similar to normal tissues and the process of automation for segmentation of MRI outputs thereby faces many challenges. One of these challenges is surmounted by utilizing prior information related to the appearance of normal body while performing classification from a multi-dimensional volumetric features set. This is tantamount in using a statistical model for tumor and normal tissue of similar features.

Presently, manual segmentation and analyses of MR images of body tumor is carried out by radiologists nearly in all hospitals. The reliability of the segmentation is entirely depends on the knowledge and skill of the radiologists. Nevertheless, this manual process is not only tedious and time-consuming but highly subjective and impractical in today's medical imaging diagnosis where a large number of images are usually taken from a single patient. It is needless to mention that the automation of the tumor detection and image segmentation process is ever demanding. Despite numerous efforts and promising results in medical imaging community the quest for efficient and precise methods is never ending. There remain many challenges such as accurate and reproducible segmentation and characterization of abnormalities using intelligent algorithms. The complexities associated with varieties of shapes, locations and image intensities of different brain tumors demand smart algorithms for detection and analyses. The need of automated body tumor detection and segmentation system from MR image is justified.

■4.0 ACTIVE CONTOUR MODELS

4.1 Definition

As mentioned before, the concept of snake was introduced by Kass *et al*. [4]. by observing the behavior active contours on a given image. While minimizing their energy, it slithers on the image. A snake is expressed as a planar parametric curve represented by,

$$\mathbf{v(s) = [x(s), y(s)]} \qquad \mathbf{s \in [0,1]} \qquad \mathbf{(1)}$$

The parameter is the snake control points called snaxels which are connected to make an active contour as shown in Figure 5. The snake is not a method for automatically detecting the boundary of the desired object in an image but requires an appropriate parameters setting and initial locations of the snaxels according to the subjective boundary. Therefore, some prior knowledge of the image from somewhat higher level system is prerequisite.

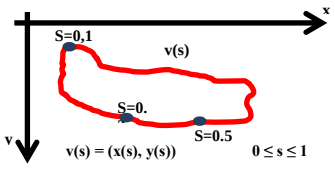

Figure 5 Parametric curve displaying snaxels in snake

The snake is defined as an energy minimizing spline that deforms itself by minimizing the energy [4]. The energy functions of a snake yields,

$$\mathbf{E_{snake}} = \int_0^1 (\boldsymbol{\alpha}.\mathbf{E_{elastic}}(\mathbf{v(s)}) + \boldsymbol{\beta}.\mathbf{E_{bending}}(\mathbf{v(s)}) + \boldsymbol{\gamma}.\mathbf{E_{image}}(\mathbf{v(s)}))\mathbf{ds} \qquad \mathbf{(2)}$$

The energy function is designed for convergence towards the boundary of the target. It acts similar to a rubber band that it put outside of an object and shirks for reaching the boundary of the target. The first two terms in Equation (2) is the internal energy which control the tension and rigidity of the snake. The third term is the external energy and is usually derived by the image that helps in attracting the snake to the target contour.

4.2 Internal Energy

The internal energy consisting of two components originating from the elasticity and bending forces is given by the expression,

$$\mathbf{E_{interal}} = \left[\boldsymbol{\alpha}(\mathbf{s})\left|\frac{\mathbf{dv(s)}}{\mathbf{ds}}\right|^2 + \boldsymbol{\beta}(\mathbf{s})\left|\frac{\mathbf{dv(s)^2}}{\mathbf{ds^2}}\right|^2\right]/\mathbf{2} \qquad \mathbf{(3)}$$

The first and second derivatives of the contour representing these energy terms are called elastic and bending forces, respectively. The elastic force helps in controlling the tension of the snake by discouraging the stretching of the active contour and remains responsible for shrinking the contour as pointed by red arrow in Figure 6.

The bending force is defined as the bending energy which allows snake acts like a thin plate [4]. It facilitates in controlling the rigidity of the snake. It also assists in controlling the curvature, without changing the length of the contour. During the deformation process it tries to maintain a smooth curve or straight line as indicated by blue-dashed arrow in Figure 6.

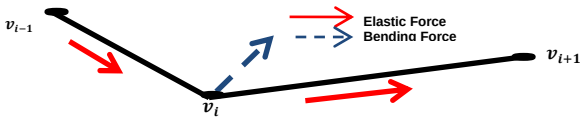

Figure 6 Variation in internal energy

The coefficients α(s) and β(s) represent constants values of weighting functions for all snaxels. Selection of an appropriate set of these constants is necessary because of their significant impact in snake's behaviors. The performance of the deformation process is entirely controlled by these constants. Each object in an image requires a different set of constants for the best performance of the snake. One way of solving this problem is to allow the snake to change dynamically for suitable values of these constants during the deformation process. This dynamical alteration necessitates a computer for automatically recognizing the shapes or topologies of an object in the image. Consequently, the solution is left for further improvements of the snake. Presently, the selection of these parameters is up to the user for initialization process.

4.3 External Energy

The external energy is obtained from the image data and it is the image-driven force that aids in attracting the snake to move toward the target contour. Following Kass et al. the expression for energies are given by [4],

$$\boldsymbol{E_{external}(s)} = -\boldsymbol{\gamma(s)}.\left|\boldsymbol{\nabla(I(s))}\right|^2 \qquad \mathbf{(4)}$$

$$\boldsymbol{E_{external}(s)} = -\boldsymbol{\gamma(s)}.\left|\boldsymbol{\nabla(G_\sigma(s) * I(s))}\right|^2 \qquad \mathbf{(5)}$$

where ∇ is the gradient operator, I(s) is the intensity of the image at s and $G_\sigma(s)$ is the two dimensional Gaussian functions with standard deviation σ, a vital feature to acquire the range of the snake. The weight function γ(s) is commonly employed to regulate the image coerce.

The Gaussian filtration system is carried out on the original image for improving the acquired range of the snake via Equation (4). This filtration system is helpful in transforming the image into blurring. Routinely, Equation (5) is used as a tool to calculate the additional force considering the square of the gradient is significantly acquires small-scale range. Higher values of σ cause blurring in the objects boundaries. Often, this is essential to make an active curve to shift towards the preferred boundary.

4.4 Snake Algorithm

Most of the snake algorithms consist of the three phases called initialization, deformation and termination as described below.

4.4.1 Initialization

During initialization, the user fits a set of the initial locations of the snaxels around the target object boundary. Meanwhile, the set of weighting parameters α, β and γ are suitably chosen so that the snake deforms itself towards the true object boundaries. The initial contour should be closer to the subject boundary since the snake can move toward noises or other unwanted edges or lines on an image if it is kept away from the true boundary.

4.4.2 Deformation

In this process, self-deformation (in each iteration) starts for minimizing the energy function given in Equation (2). Corresponding to each snaxel, a new location is searched among neighboring pixels. A snaxel moves to a pixel if a lower energy configuration is available otherwise it remains in the same location. Two approaches are offered to compute new locations for snaxels in which the greedy algorithm is commonly used due to its simplicity and easy implementation.

During the iterations, the sum of the internal and external energies is computed at a snaxel and its eight neighboring pixels. The location having lower energy is preferred to be a new location. Hence, a snaxel starts moving to one of the eight possible neighboring pixels as displayed by red arrows in Figure 7. Otherwise, it remains in the same location due the absence of lower energy configuration.

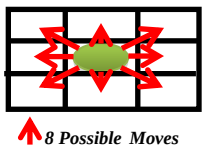

Figure 7 The greedy algorithm for deformation process of active contour

4.4.3 Termination

Sometimes the deformation of the snake needs to be terminated. Naturally, the deformation is ceased if all the snaxels fail to find new locations in the neighboring pixels. Simply, it converges to zero and disappears from the sight. However, it may end up in an infinite loop when the snaxels are shifted along the boundary or some of snaxels oscillate. Thus, some termination criteria of the snake are inevitable. A simpler way to terminate is to set a threshold on the maximum number of iterations executed in the deformation process. This guarantees that the snake is terminated and it never ends up in an infinite loop. However, the user needs to set the appropriate number of iterations before the deformation process starts. Indeed, it is difficult to estimate the number of required iterations for detecting the subject contour because the numbers greatly vary depending on the shape and the size of the target object. However, setting the smaller number of the maximum iterations assures the snake gets terminated either before reaching or closer to the true boundary.

The terminating criteria in this case are not useful because sometimes the snaxels gets shifted along the boundary and the contour only moves very slightly.
Frequently, the snaxels are transferred towards the boundary along with curve that merely moves [27].

■5.0 ACTIVE CONTOUR IN MRI SEGMENTATION

The segmentation of anatomic structures is essential for the first stage of most medical image analysis tasks including registration, labeling and motion tracking. These tasks require the anatomic structures in the original image to be reduced to a compact and analytic representation in their shapes. Performing this segmentation manually is extremely laborious and time-consuming. A primary example is the segmentation of the heart, especially the Left Ventricle (LV) from cardiac imagery. Segmentation of the LV is a prerequisite for computing diagnostic information such as ejection-fraction ratio, ventricular volume ratio and heart output as well as wall motion analysis which provides information on wall thickening [28]. Compared to the threshold, the active contour algorithms are more flexible and can be used for complex segmentations as displayed in Figure 8.

The model evolution is usually driven by a global energy minimization process, where the internal and external energies (corresponding to the smoothness and image forces) are integrated into a model of total energy. The optimal position/configuration is obtained in minimizing the total energy. Moreover, the initialization far away from object boundary may trap in local energy minima caused by spurious edges and/or high noise.

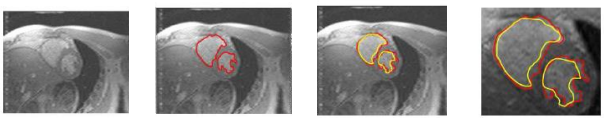

Figure 8 Segmentation of the left and right ventricles (LV, RV) in a cardiac MRI using parametric deformable models (active contours) (a) Original image, (b) Ground truth boundaries, (c) Ground-truth (red) and final solution (yellow) and (d) Magnified view of LV and RV with ground-truth and the final solution [28]

Parametric or explicit deformable models also called active contours use parametric curves to represent the model shape [4, 17, 29, 30]. Edge-based parametric models use edges as image features which usually make them sensitive to noise. Conversely, the region-based methods use region information to drive the curve [31-33]. A limitation of the latter is that they do not update the region statistics during the model evolution and therefore, local feature variations are difficult to be captured. Florin *et al.* proposed Region updating where an active contour with particle filtering is used for vascular segmentation [34].

The image in Figure 8 shows a magnification of the ventricles. One can observe that the deformable model converges

to edges that do not correspond to the actual region boundaries, which is caused by a local minimum of the model's energy.

Malladi, *et al*. and Caselles, *et al*. first applied the level set methods in medical images. Malladi's model used the gradient information as a stop criterion in which the speed is intuitive. An increase in gradient magnitude decreases the speed and thereby slows down the contour as it moves to the structure boundary. However, the model suffers from leakage due to its mere dependence on the gradient magnitude [35, 36]. Unlike Malladi's model, Geodesic Active Contour (GAC) algorithm treats the segmentation as an optimization problem for finding the minimal distance curve [37, 38]. The moving equation of GAC is also derived from energy function. Instead of directly solving the moving equation, the contour is embedded in a level set function and the moving equation then becomes a level set equation. GAC algorithm shows a strong correlation between parametric and geometric models. The introduction of level set representation in geodesic active model makes the algorithm flexible in handling the topological changes. The basic geodesic deformable snake algorithms are applied to MR, CT and ultrasound images for tumor detection and cardiac segmentation [39]. Another popular geometric model is due to paragios which is based on a simplified version of Mumford-Shah energy model [40]. The Chan-Vese's algorithm is highly advantageous in obtaining a boundary of discrete points useful for medical image applications when the interested structures are represented by discrete pixel clusters and without clear definition of boundaries.

Many efforts are dedicated to segment structures in 2D images [41, 46]. Typically, users initialized a deformable model near the object of interest and allowed it to deform to take place. The interactive capabilities of these models with manual fine-tuning are possible. Furthermore, with a satisfied result on an initial image slice, the fitted contour model can be used as the initial boundary approximation for neighboring slices. These models are then deformed and propagated until all slices have been processed. The resulting sequence of 2D contours can then be connected to form a continuous 3D surface model [47, 48]. The application of snakes and other similar deformable contour models to extract regions of interest is, however, not without limitations.

In non-interactive models initialization must be close to the structure of interest to guarantee superior performance. The internal energy constraints of snakes can limit their geometric flexibility and prevent them from representing long tube-like shapes with significant protrusions or bifurcations. Since the classical deformable contour models are parametric and are incapable of topological transformations without additional machinery, the topology of the structure of interest must be known in advance. Using simulated annealing, Poon *et al*. minimized the energy of active contour models for producing global solutions that allowed the incorporation of non-differentiable constraints [49]. They also used a discriminant function to incorporate region based image features into the image forces of their active contour model. The discriminant function allowed the inclusion of additional image features in the segmentation and served as a constraint for global segmentation consistency in which every image pixel contributed. The use of such function results in much robust energy function and better tolerance to the deviation of the initial guess from the true boundaries. In an attempt to decrease the sensitivity to insignificant edges and initial model placement, others researchers have also integrated region-based information into deformable contour models [50-52]. Recently, topology independent shape modeling schemes are developed that allows a deformable contour or surface model to not only represent long tube-like shapes with bifurcations, but also to dynamically sense and change its topology [53].

6.0 CONCLUSION

We reviewed the present status and future scopes of active contour segmentation models implemented in MRI. Salient features of different models, their advantages and limitations are compared. The insight of the importance and urgent necessity of image segmentation algorithm in tumor detection are discussed and analyzed. The need of intelligent algorithms for automated MRI segmentation to characterize tumor abnormalities in an accurate and reproducible fashion is emphasized. The increasing demand of medical imaging in the diagnosis and treatment of diseases has opened an array of multifaceted problems. The concrete medical image segmentation task boils down in combining the application background and practical requirements to design smarter and proper algorithms. Accuracy, complexity, efficiency and interactivity of a segmentation algorithm are the relevant factors need to be considered. Active contour models offer attractive approach in tackling varieties of problems due to their capability of representing the complex shapes and broad shape variability of anatomical structures. Snakes are able to overcome many limitations of traditional low-level image processing techniques and provide compact and analytical depictions of object shape, incorporate anatomic knowledge and include interactive capabilities. The continuous development and refinement of deformable models will remain an important domain of research into the foreseeable future.

Acknowledgement

Mohammed Sabbih Hamoud Al-Tamimi is grateful to the Ministry of Higher Education & Scientific Research, Iraq for providing sponsorship to continue his PhD.

References

[1] *http://www.radiologyassistant.nl/*. Accessed on: January, 12, 2012.
[2] Louis D. N., Ohgaki H., Wiestler O. D., Cavenee, W. K. (Eds.). 2007. *Classification of Tumors of the Central Nervous System*, (IARC), Lyon.
[3] Alpert, S., Galun, M., Basri, R., and Brandt, A. June 2007. Image Segmentation by Probabilistic Bottom-up Aggregation and Cue Integration. In Computer Vision and Pattern Recognition, IEEE Conference. 1–8.
[4] M. Kass, A. Witkin, and D. Terzopoulos. 1987. Snakes-active Contour Models. *Int. J. Computer. Vis.* 1: 321–33.
[5] D. Terzopoulos, A. Witkin, and M. Kass. 1988. Constraints on Deformable Models-recovering 3D Shape and Nonrigid Motion. *Art. Intel.* 36: 91–123.
[6] M. Gastaud, M. Barlaud, and G. Aubert. May 2004. Combining Shape Prior and Statistical Features for Active Contour Segmentation. *IEEE Trans. Circuits Syst. Video Technol.* 14(5): 726–734.
[7] J.-O. Lachaud and A. Montanvert. 1999. Deformable Meshes with Automated Topology Changes for Coarse-to-Fine Three-dimensional Surface Extraction. *Med. Image Anal.* 3: 187–20.
[8] T. McInemey and D. Terzopoulos. Oct. 1999. Topology Adaptive Deformable Surfaces for Medical Image Volume Segmentation. *IEEE Trans. Med. Image.* 18(10): 840–850.
[9] T. McInerney and D. Terzopoulos. 1995. A Dynamic Finite Element Surface Model for Segmentation and Tracking in Multidimensional Medical Images with Application to Cardiac 4D Image Analysis. *Computer Med. Image Graph*. 19: 69–83.
[10] N. Ray and S. T. Acton. Dec. 2004. Motion Gradient Vector Flow: An External Force for Tracking Rolling Leukocytes with Shape and Size Constrained Active Contours. *IEEE Trans. Med. Image*. 23(12): 1466–1478.

[11] N. Ray, S. T. Acton, and K. Ley. Oct. 2002. Tracking Leukocytes in Vivo with Shape and Size Constrained Active Contours. *IEEE Trans. Med. Image*. 21(10): 1222–1235.
[12] A. R. Mansouri, D. P. Mukherjee, and S. T. Acton. Jun. 2004. Constraining Active Contour Evolution via Lie Groups of Transformation. *IEEE Trans. Image Process*. 13(6): 853–863.
[13] N. Paragios and R. Deriche. Mar. 2000. Geodesic Active Contours and Level Sets for the Detection and Tracking of Moving Objects. *IEEE Trans. Pattern Anal. Mach. Intell.* 22(3): 266–280.
[14] T. F. Cootes, G. J. Edwards, and C. J. Taylor. Jun. 2001. Active Appearance Models. *IEEE Trans. Pattern Anal. Mach. Intell*. 23(6): 681–685.
[15] T. F. Cootes, C. J. Talyor, D. H. Cooper, and J. Graham. 1995. Active Shape Models-Their Training and Applications. *Computer Vis. Image Understand.* 61: 38–59.
[16] J. A. Sethian. 1999. *Level Set Methods and Fast Marching Methods: Evolving Interfaces in Computational Geometry, Fluid Mechanics, Computer Vision, and Materials Science*. U.K.: Cambridge Univ.
[17] D. Terzopoulos and T. McInerey. 1996. Deformable Models in Medical Image Analysis: A Survey. *Med. Image Anal.* 1: 91–108.
[18] Damadian, R., Goldsmith, M. & Minkoff, L. 1977. NMR in Cancer: XVI. FONAR Image of the Live Human Body. *Physiological Chemistry and Physics*. 9(1): 97–100, ISSN: 0031-9325.
[19] Novelline, R. A. & Squire, L. F. 2004. *Squire's Fundamentals of Radiology*. Harvard Univ. Press. ISBN 0674012798
[20] A. O Rodriguez. 2004. *Principles of Magnetic Resonance Imaging.* 50(3): 272–286.
[21] *www.teamrads.com/Cases/Neuroanatomy/MRI*. Accessed on: January, 2012.
[22] C. Westbrook. 2002. *MRI at Glance*. Blackwell Science Publishing.
[23] Prima, S., Ayache, N., Barrick, T. & Roberts, N. 2001. Maximum Likelihood Estimation of the Bias Field in MR Brain Images: Investigating Different Modeling of the Imaging Process. *Processing of Medical Image Computing and Computer-Assisted Intervention*. 2208: 811–819.
[24] Li, X., Li, L., Lu, H., Chen, D. & Liang, Z. 2003. *Inhomogeneity Correction for Magnetic Resonance Images with Fuzzy C-Mean Algorithm*. Proc. of SPIE. 5032.
[25] Ruan, S., Jaggi, C., Xue, J., Fadili, J. & Bloyet, D. 2000. Brain Tissue Classification of Magnetic Resonance Images Using Partial Volume Modeling. *IEEE Trans. Medical Imaging*. 19(12): 1179–1187.
[26] W. Choi, K. Lam and W. Siu. 2001. An Adaptive Active Contour Model for Highly Irregular Boundaries. *Pattern Recognition.* 34: 323–331.
[27] A. Singh, L. von Kurowski, and M. Chiu. 1993. Cardiac MR Image Segmentation Using Deformable Models. In Biomedical Image Processing and Biomedical Visualization. 1905*:* 8–28.
[28] L. D. Cohen and I. Cohen. 1993. Finite-element Methods for Active Contour Models and Balloons for 2-D and 3-D Images. *IEEE Trans. on Pattern Analysis and Machine Intelligence*. 15: 1131–1147.
[29] C. Xu and J. L. Prince. 1998. Snakes, Shapes and Gradient Vector Flow. IEEE Trans. on Image Processing. 7(3): 359–369.
[30] R. Ronfard. 1994. Region-based Strategies for Active Contour Models. *Int'l Journal of Computer Vision*. 13(2): 229251.
[31] S. Zhu and A. Yuille. 1996. Region Competition: Unifying Snakes, Region Growing, and Bayes/MDL for Multiband Image Segmentation. IEEE Trans. on Pattern Analysis and Machine Intelligence. 18(9): 884–900,
[32] R. Huang, V. Pavlovic, and D. Metaxas. 2004. A Graphical Model Framework for Coupling MRFs and Deformable Models. IEEE Conf. on Computer Vision and Pattern Recognition.
[33] C. Florin, J. Williams, and N. Paragios. 2006. Globally Optimal Active Contours, Sequential Monte Carlo and On-line Learning for Vessel Segmentation. European Conf. on Computer Vision.
[34] Malladi, R., Sethian, J. A., Vemuri, B. 1993. A Topology Independent Shape Modeling Scheme. SPIE Conf. on Geometric Methods in Computer Vision II. 2031: 246–58.
[35] R. Malladi, J. Sethian, and B. Vemuri. 1995. Shape Modeling with Front Propagation: A Level Set Approach. *IEEE Trans. on Pattern Analysis and Machine Intelligence*. 17(2): 158–175.
[36] Caselles, V., Kimmel, R., Sapiro, G. 1997. Geodesic Active Contours. *Int. J. of Comp. Vision*. 22: 61–79.
[37] T. Jones and D. Metaxas. 1997. Automated 3D Segmentation using Deformable Models and Fuzzy Affinity. Information Processing in Medical Imaging.
[38] Chan, T., Vese, L. A., 1999. An Active Contour Without Edge. Int. Conf. Scale-Space Theories in Computer Vision. 141–151.
[39] Paragios, N. 2002. A Variational Approach for the Segmentation of the Left Ventricle in Cardiac Image Analysis. *International Journal of Computer Vision*. 50: 345–62.
[40] N. Rougon and E Preteux. 1993. Directional Adaptive Deformable Models for Segmentation with Application to 2D and 3D Medical Images. In Medical Imaging 93; Image Processing, volume 1898. 193–207. Bellingham, WA.
[41] Carlbom, D. Terzopoulos, and K. Harris. 1994. Computer Assisted Registration, Segmentation, and 3D Reconstruction from Images of Neuronal Tissue Sections. *IEEE Trans. On Medical Imaging*. 13(2): 351–362.
[42] A. Gupta, T. O'Donnell, and A. Singh. Sep. 1994. Segmentation and Tracking of Cine Cardiac MR and CT Images using a 3-D Deformable Model. In Proc. IEEE Con. on Computers in Cardiolog.
[43] S. Lobregt and M. Viergever. March 1995. A Discrete Dynamic Contour Model. *IEEE Trans. on Medical Imaging*. 14(1): 12–24.
[44] G. Tsechpenakis, B. Lujan, O. Martinez, G. Gregori, and P.J. Rosenfeld. Sept. 2008. Geometric Deformable Model Driven by CoCRFs: Application to Optical Coherence Tomography. Int'l Conf. on Medical Image Computing and Computer Assisted Intervention, NYC, NY.
[45] G. Tsechpenakis, and D. Metaxas. 2007. CRF-driven Implicit Deformable Model. IEEE Conf. on Computer Vision and Pattern Recognition.
[46] L. Chang, H. Chen, and J. Ho. July 1991. Reconstruction of 3D Medical Images: A Nonlinear Interpolation Technique for Reconstruction of 3D Medical Images. *Computer Vision, Graphics, and Image Proc*. 382–391.
[47] G. Tsechpenakis, J. Wang, B. Mayer, and D. Metaxas. 2007. Coupling CRFs and Deformable Models for 3D Medical Image Segmentation. *IEEE Mathematical Methods in Biomedical Image Analysis*.
[48] C. S**.** Poon, M. Braun, R. Fahrig, A. Ginige, and A. Dorrell. Segmentation of Medical Images Using an Active Contour Model Incorporating Region-based Images Features. In Robb.
[49] N. Rougon and E Preteux. 1991. Deformable Markers: Mathematical Morphology for Active Contour Models Control. In Image Algebra and Morphological Image Processing 11. 1568: 78–89. Bellingham.
[50] I. Herlin, C. Nguyen, and C. Graffigne. June 1992. A Deformable Region Model Using Stochastic Processes Applied to Echocardiographic Images. In. CVPR 921. 534–539. Los Alamitos, IEEE Computer Society Press.
[51] J. Gauch, H. Pien, and J. Shah. Hybrid. 1994. Boundary-based and Region-based Deformable Models for Biomedical Image Segmentation. In Mathematical Methods in Medical Imaging. 2299: 72–83.
[52] G. Sapiro, R. Kimmel, and V. Caselles. 1995. Object Detection and Measurements in Medical Images Via Geodesic Deformable Contours. In Vision Geometry IV. 2573: 366–37.